

⁹S. N. Vlasov, L. V. Piskunova, and V. V. Talanov, *Zh. Eksp. Teor. Fiz.* **75**, 1602 (1978) [*Sov. Phys. JETP* **48**, 808 (1978)].
¹⁰S. A. Akhmanov, A. P. Sukhorukov, and R. V. Khokhlov, *Usp. Fiz. Nauk* **93**, 19 (1967) [*Sov. Phys. Usp.* **10**, 609 (1968)].
¹¹R. Y. Chiao, E. Garmire, and C. H. Townes, *Phys. Rev. Lett.* **13**, 479 (1964).

¹²V. I. Talanov, *Pis'ma Zh. Eksp. Teor. Fiz.* **11**, 303 (1970) [*JETP Lett.* **11**, 199 (1970)].
¹³V. I. Bespalov and V. I. Talanov, *Pis'ma Zh. Eksp. Teor. Fiz.* **3**, 471 (1966) [*JETP Lett.* **3**, 307 (1966)].

Translated by J. G. Adashko

Measurement of ionization threshold intensities in helium using ponderomotive force accelerated electrons

B. W. Boreham and J. L. Hughes

Photon Physics Group, Dept. of Engineering Physics, The Australian National University, Canberra, Australia
(Submitted 14 May 1980)
Zh. Eksp. Teor. Fiz. **80**, 496-511 (February 1981)

The results of an experimental program to study the ionization of atoms by intense laser beams are presented. New experimental results concerning the distribution of photo-electrons as a function of their energy and the dependence of electron emission on laser beam intensity for values up to 6×10^{16} W/cm² have been obtained.

PACS numbers: 32.80.Fb

1. INTRODUCTION

Accurate knowledge of both the electric field intensities and the time at which ionization occurs in any test gas volume is essential to a number of the projects involving the interactions of intense laser beams with matter. These include self-focusing¹ and ionization of dense plasmas by intense laser beams² and the ionization and radiation-matter interaction studies in tenuous plasmas³⁻⁵, as well as the study of possible photon fission processes within intense laser beams enveloped by intense Coulomb fields.⁶

In the experiments discussed here the number and integrated energy spectra^{3,4} of electrons emitted by the action of ponderomotive force from the focus region of a high intensity neodymium laser beam focused into a tenuous helium plasma were measured as a function of the laser intensity over the range 10^{14} to 6×10^{16} W/cm².

The energy spectra were found to be characteristic of electrons accelerated by ponderomotive forces.^{3,5} The spectral profiles are independent of laser intensity, but strongly dependent on the degree of ionization of the test gas. Measurement of the intensities at which spectral shape changes occur provides a means of obtaining the ionization threshold intensities for any test gas. Alternatively these threshold intensities will be obtained more accurately as the asymptotic values of curves of the number of electrons against intensity with electron energy as a parameter. Both types of measurement were carried out and the results compared with values calculated using the general formula for ionization probability as given by Keldysh.⁷

2. APPARATUS

The laser system consisted of a passively mode-locked Nd:YAG oscillator producing trains of individual pulses with a nominal duration equal to 25 psec. Single pulses from the oscillator were isolated using a pair

of tandem-connected Pockel's cells with an overall contrast ratio greater than 10^4 , and then amplified to a level of about 1 joule using Nd:YAG and Nd:Glass amplifiers. A single-vacuum spatial filter was also included within the amplifier chain to keep the value of the beam break-up integral low and thereby ensure that the beams focusing properties were not adversely affected by refractive index non-linearly within the laser glass.

Measurements have shown a significant fluctuation in the pulse duration from the oscillator⁸ with 80% of pulses having durations between 18-36 psec and 60% between 20 and 30 psec. The duration of individual pulses used in the experiments was measured using a two-photon fluorescence monitor to an accuracy of better than 10%.

As illustrated in Fig. 1, the beam was focused using a 75 mm aspheric lens inside an evacuated chamber which had subsequently been filled with helium gas to a pressure of 10^{-4} Torr after evacuation to less than 5×10^{-7} Torr. The distribution of power in the focused beam was measured in a separate experiment by ablating an aluminum film off a glass substrate which was placed in the beam.⁵

The electrons emitted from the focal region were collected over a solid angle of 2.7 sr by a multidirectional retarding-field electron energy analyzer. This detector was constructed from four monodirectional retarding-field electron-energy analyzers, one of which is illustrated in Fig. 1. Grids 1 and 3 were grounded and grid 2 acted as a retarding grid which was negatively biased to prevent electrons with energies less than the grid potential from reaching the collector. The collector itself was biased to +45 volts to prevent secondary electron losses.

The minimum charge which could be detected was $\sim 10^{-15}$ Coulombs, which is equivalent to a detection

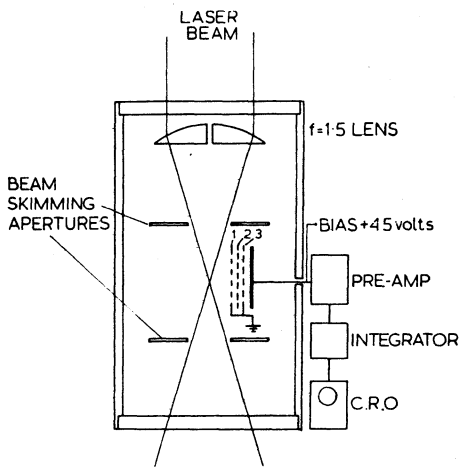


FIG. 1. Experimental apparatus—the vacuum base pressure was less than 5×10^{-7} Torr.

level $\sim 6 \times 10^3$ electrons. A consequence of this detection threshold is that electrons generated in the very highest intensity regions of the beam will not be detected. For example, at a pressure of 10^{-4} Torr the volume of fully ionized gas must exceed 2.3×10^{-9} cm³ before any ionization electrons can be detected, assuming that all the emitted electrons are detected. However, since the detector did not completely surround the focal volume, more free electrons must be emitted before the minimum charge is detected. This requires the production of $\sim 1.8 \times 10^4$ electrons in the focal region, corresponding to a fully singly ionized volume 5.6×10^{-9} cm³ at 10^{-4} Torr. Analysis of the power distribution in the focal region⁵ indicates that the intensity will have fallen to 0.64 of the peak intensity on the surface enclosing this minimum volume.

The detector was shielded from stray electrons originating at the lens or entrance window surfaces by the beam skimming apertures shown in Fig. 1. Signal levels from these sources and from the residual gas in the chamber were found to be negligible.

Measurements were made also of the total electron yields as a function of the helium pressure, laser intensity, and retarding grid potential. The results are presented in Figs. 6 to 10.

3. THEORY

The method relies on measurement of the energy of ionization electrons which are accelerated from the beam by the non-linear ponderomotive force,⁵ produced by the strong electric field gradient in the laser focus volume

$$f_{NL} = \frac{-e^2}{4m_e \omega^2} \nabla |E|^2, \quad (1)$$

where E is defined by $\mathbf{E}_s(\mathbf{r}) = \mathbf{E}(\mathbf{r}) \cos \omega t$ and \mathbf{r} is the positional vector.

In the high intensity limit (in which the electron is accelerated instantaneously from the beam)^{4,5,9} the average kinetic energy of the maximum oscillation of

the electrons in the alternating field, $\epsilon_{kin,e}^{osc}$, is converted to a final directed kinetic energy, ϵ_e^{trans} , i. e.,

$$\epsilon_e^{trans} = \epsilon_{kin,e}^{osc} = \epsilon_e^{osc} / 2 = e^2 E^2 / 4m_e \omega^2, \quad (2)$$

where ϵ_e^{osc} is the total oscillation energy. For Nd glass equation (2) gives

$$\epsilon_e^{trans} \sim 10^{-12} I, \quad (3)$$

where ϵ is in eV and I is in W/cm². This equation is valid for laser intensities greater than $I \sim 10^{13}$ W/cm².

It is seen from Eq. (3) that electrons produced by ionization at a particular laser intensity will be ejected from the focal region with a characteristic energy that depends on that intensity, and in certain conditions measurement of the ejected electron energy can be used to determine the ionization threshold.

A general expression for the probability of ionizing atoms and solid bodies in the field of a strong electromagnetic wave that takes into account the acceleration of the free electron in the oscillating field to an average energy has been obtained by Keldysh.⁷ In the simplest case of ionization of atoms the general formula for the ionization probability is

$$W = A \omega \left[\frac{\chi_0}{\hbar \omega} \right]^{1/2} \left[\frac{\gamma}{(1+\gamma^2)^{1/2}} \right]^{1/2} S \left(\gamma, \frac{\tilde{\chi}_0}{\hbar \omega} \right) \times \exp \left\{ - \frac{2\tilde{\chi}_0}{\hbar \omega} \left[\text{Arsh } \gamma - \gamma \frac{(1+\gamma^2)^{1/2}}{1+2\gamma^2} \right] \right\}, \quad (4)$$

where ω is the frequency and χ_0 the ionization potential of the gas. The effective ionization potential is defined by:

$$\tilde{\chi}_0 = \chi_0 + e^2 E^2 / 4m_e \omega^2 = \chi_0 (1 + 1/2\gamma^2)$$

(where E is the electric field strength);

$S(\gamma, \tilde{\chi}_0/\hbar \omega)$ is a relatively slowly varying function of the frequency and of the field: A is a numerical constant; $\gamma = \omega(2m_e \chi_0)^{1/2} / eE$.

Under specific conditions Eq. (4) is reducible to two limiting cases. At high frequencies and moderate fields ($\gamma \gg 1$) a multiphoton absorption formula is obtained. In the opposite case of low frequencies and very strong fields ($\gamma \ll 1$) a tunnel-effect formula is obtained. In the experiments described in this paper it is the latter formula that is assumed to apply, since γ varies over the range ~ 0.6 to 0.1 . The formula reduces to

$$W_0 = \frac{A(6\pi)^{1/2} \chi_0}{4} \frac{1}{\hbar} \left[\frac{eE\hbar}{m_e^{1/2} \chi_0^{1/2}} \right]^{1/2} \exp \left\{ - \frac{4}{3} \frac{(2m_e)^{1/2}}{e\hbar E} \chi_0^{1/2} \times \left[1 - \frac{m_e \omega^2 \chi_0}{5e^2 E^2} \right] \right\} \quad (5)$$

or in cgs. esu units

$$W_0 = 1.44 \cdot 10^{12} A [I \chi_0]^{1/2} \exp \{ -2.5 \cdot 10^{16} [\chi_0/I]^{1/2} (1 - 4.78 \cdot 10^{14} \chi_0/I) \}, \quad (6)$$

where I is the laser intensity in units of W/cm², χ_0 is in eV, A is assumed to have a value of order 1, and W_0 is in sec⁻¹.

It has been suggested⁹ that Eq. (5) should be corrected further to account for Coulomb interaction in the final state. Keldysh⁸ introduced an appropriate correction factor $\gamma_0 \gamma / \hbar \omega (1 + \gamma^2)^{1/2}$. When this is included,

(5) and (6) become

$$W_0 = A \left[\frac{m_e \chi_0^7}{e^2 E^2 \hbar^6} \right]^{1/4} \exp \left[-\frac{4}{3} \frac{(2m_e)^{1/2} \chi_0^{3/2}}{e E \hbar} \left(1 - \frac{m_e \omega^2 \chi_0}{5e^2 E^2} \right) \right], \quad (5a)$$

$$W_0 = 2.28 \cdot 10^{19} (\chi_0^7 / I)^{1/4} \exp [-2.5 \cdot 10^{16} (\chi_0^3 / I)^{1/2} (1 - 4.78 \cdot 10^{14} \chi_0 / I)]. \quad (5a)$$

(where A has been assumed to be 13, which is the value that produces good agreement with other tunneling expressions for the hydrogen atom). It will be shown that the choice of A is not critical, as the ionization probability changes by several orders of magnitude for a change of only 20% in intensity, and varying A by several orders of magnitude changes the final result by the order of 20%.

Correction for the long range nature of the Coulomb potential does not result in a change in the value of γ^2 which marks the boundary between the multiphoton and tunneling regimes.¹⁰

A computer program was formulated to solve Eqs. (5) and (5a) for both the ionization threshold intensity (i. e., the minimum intensity for which the integral of W_0 with respect to time equals unity and the ionization time when the intensity exceeds the threshold. The results of these calculations are shown in Figs. 2 to 5.

Figure 2 is a plot of ionization threshold intensity as a function of ionization potential for laser pulses with both square and Gaussian profiles in time, each corrected and uncorrected for Coulomb effects. For the Gaussian pulse the ionization intensity is defined to be equal to the peak pulse intensity and the pulse width is 25 psec. Figure 3 illustrates the rapid change in the ionization probability, for relatively small changes in laser intensity. for the case of helium and a Gaussian pulse, again corrected and uncorrected for Coulomb effects.

The time at which ionization will occur in a helium

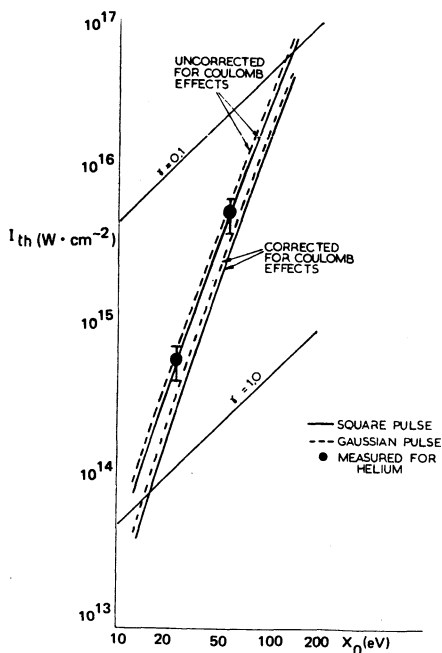


FIG. 2. Ionization threshold intensity as a function of ionization potential.

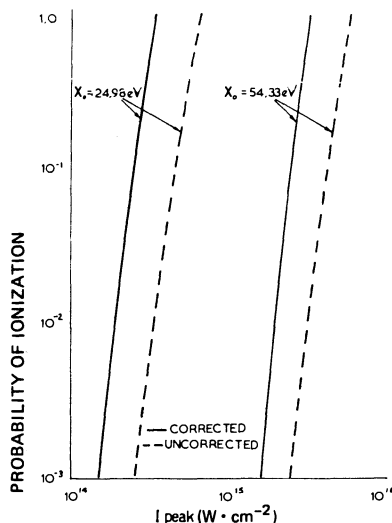


FIG. 3. Probability function behavior.

test gas irradiated by a time-dependent Gaussian pulse is given as a function of the pulse peak intensity in Fig. 4. The probability function has been integrated relative to time zero corresponding to the peak of the pulse; τ' is the ionization time relative to the time value at the negative $1/e$ intensity value (i. e., -12.5 psec for a 25 psec pulse width) and τ'' is the ionization time relative to twice the time corresponding to the negative $1/e^2$ intensity value (i. e., -35.4 psec for a 25 psec pulse width). The extremely rapid decrease in ionization time with increasing peak intensity results from the very rapid onset of ionization that would be expected from the ionization probability curves of Fig. 3, which are closely approximated by a linear function. It is seen also that the ionization times are several orders of magnitude greater than ω^{-1} . This result can again be anticipated from Fig. 3, which shows that the integrated contribution to the ionization probability will be negligible until the intensity has risen to a value that closely approaches that at which ionization occurs. Ionization then occurs extremely rapidly.

The solution convergence is illustrated in Fig. 5 for a Gaussian curve with 25 psec pulse width. The lower

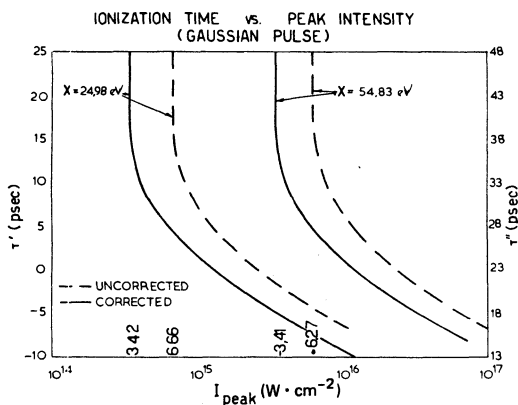


FIG. 4. Ionization time as a function of peak laser pulse intensity.

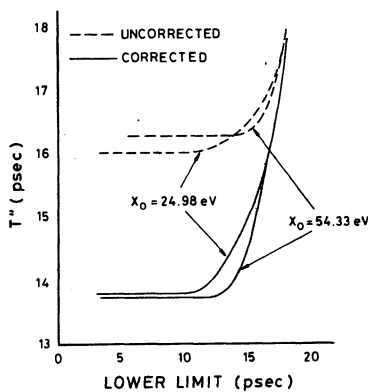


FIG. 5. Solution convergence for $\chi_0 = 24.98$ eV and $\chi_0 = 54.33$ eV.

integration limit is arbitrarily set at a value between -17.7 and -35.4 psec and the integration proceeds until an upper limiting value that gives an ionization probability if unity is found. This upper limit is defined as the ionization time and is plotted in Fig. 5 against the lower integration limit, taken relative to -35.4 psec. In both cases convergence occurs well before -35.4 psec, and at lower peak intensities convergence is even more rapid.

Once the ionization time is determined (from Fig. 4), the intensity at which ionization occurs is also known and Eq. (3) can be used to predict the energies with which electrons from the two different ionization states of helium will be observed. As the laser intensity is increased, the onset of the second state will be marked by the appearance of electrons with higher energies, corresponding to the higher threshold intensity. The integrated electron spectra (number of electrons with energy greater than the retarding grid potential as a function of that potential), as obtained with the retarding energy analyzer, can therefore be used to differentiate between these two states.

4. RESULTS AND DISCUSSION

In Fig. 6 the total electron signal for zero retarding grid potential is plotted as a function of peak laser intensity (calculated in the focal plane). Also shown are the total calculated signals expected for first ionization threshold intensities in helium ($\chi_0 = 24.98$ eV) of 3.42×10^{14} W/cm² and 6.66×10^{14} W/cm² which are the calculated values for ionization with a Gaussian pulse corrected and uncorrected for Coulomb effects respectively, as seen from Fig. 3. (This calculation was carried out by integration in order to obtain the volume enclosed by the various beam intensity contours as obtained from the experimentally determined power distribution in the focused beam.)

The measured values fall between the calculated limits although agreeing more closely with the uncorrected first ionization threshold value of 6.66×10^{14} W/cm², up to intensities of the order of 6×10^{15} W/cm². The minimum intensity at which electrons were detected was $(8.2 \pm 0.4) \times 10^{14}$ W/cm², which gives an ionization threshold of $(5.2 \pm 0.3) \times 10^{14}$ W/cm². (For comparison, the multiphoton ionization threshold has been calculated¹²

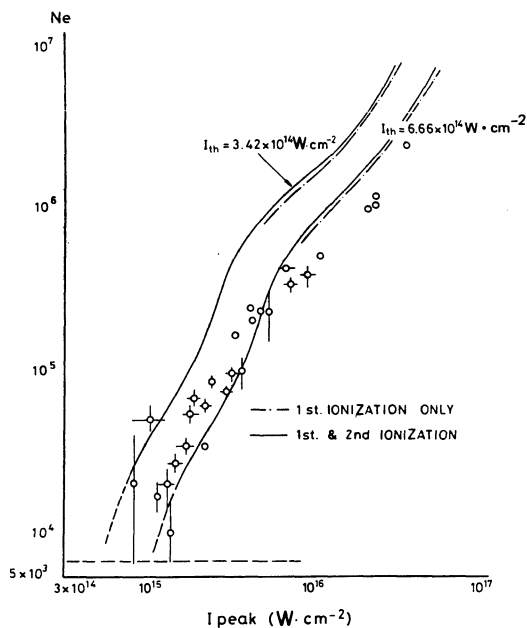


FIG. 6. Electron yield as a function of laser peak intensity.

using the Keldysh formula in the multiphoton limit as approximated by Raizer¹². The value obtained as 3.6×10^{14} W/cm².)

At intensities above the order of 6×10^{15} W/cm², the measured values fall away from the calculated curve. This may be caused by secondary electron emission but a more likely reason is some form of collective photon effect at high intensities imposing an axial velocity component on the electrons and thus preventing some of them from reaching the detector, or electron loss due to trapping of electrons in intensity wells in the focus region.

Measurement of the equal-intensity contours in the focal region have shown⁵ that in the focal plane the beam has an approximately Gaussian profile, whilst away from the focus the intensity distribution becomes more complicated with regions of peak intensity occurring off axis for high intensity ratios. These peaks will prevent some electrons from being accelerated in the radial direction and instead they will be accelerated in the axial direction by the normally negligible component of the ponderomotive force and will not be detected. This effect will first become detectable when the laser intensity is approximately an order of magnitude greater than the threshold intensity and will become rapidly more significant as the intensity is further increased.

An estimate of the number of electrons that will be lost in this manner as a function of the laser intensity has been made and the total calculated electron signal expected when this loss is accounted for is shown in Fig. 7 where the ionization threshold intensity has been assumed to be 5.2×10^{14} W/cm². It is seen that when this loss is considered, good agreement is obtained between the calculated and measured signals. A further correction can be made for the small effect of Coulomb coupling between the electrons and the posi-

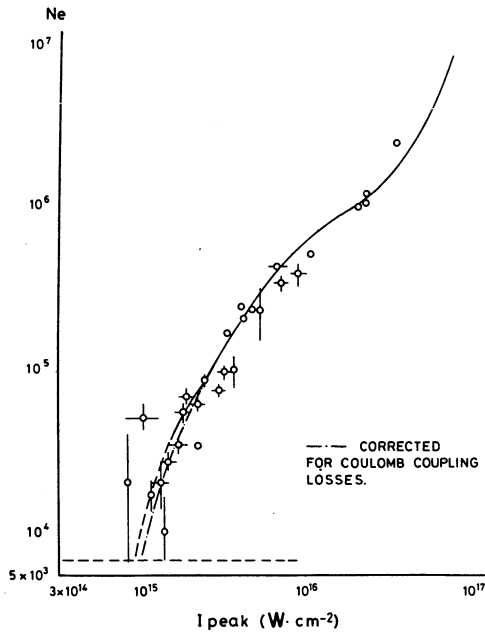


FIG. 7. Electron yield compared with the calculated yield assuming a threshold intensity of $5.2 \times 10^{14} \text{ W/cm}^2$.

tive ions^{4,13} and the result of this correction is also shown in Fig. 7. The agreement is seen to be further improved.

The increase of the measured value of N_e with intensity as shown in Figs. 6 and 7, is due to the increase in the size of ionization volume within the focal region. It is seen that the fluctuations in the value of N_e follow the fluctuations in the ionization volume, emphasizing the fact that saturation has been achieved and therefore all the photons are involved in the ionization process.

Also shown in Fig. 6 is the calculated contribution made to the total number of detected electrons by second ionization electrons. This contribution is seen to be smaller than the errors in the measured values, and hence second-ionization electrons would not be expected to be detected on this curve. The energy of these electrons is large, however, as they come from the high intensity central beam region and they may therefore be detected by increasing the retarding grid potential until the first-ionization electrons are prevented from reaching the detector.

In Fig. 8 the electron signal is plotted as a function of retarding grid potential with peak intensity as a parameter. At higher intensities a distinct slope change is observed in the integrated electron spectra indicating the presence of a smaller number of higher-energy electrons, as would be expected when second-ionization electrons were present. It is seen that the second-ionization electrons first appear within the intensity range of $(8.8 \pm 1.3) \times 10^{15} \text{ W/cm}^2$ and $(1.1 \pm 0.2) \times 10^{16} \text{ W/cm}^2$, which agrees well with the value of $9.8 \times 10^{15} \text{ W/cm}^2$ calculated for a threshold intensity $6.27 \times 10^{15} \text{ W/cm}^2$, a detection limit 1.8×10^4 electrons, and an ionization potential 54.83 eV.

In Fig. 9 the maximum detectable electron energies

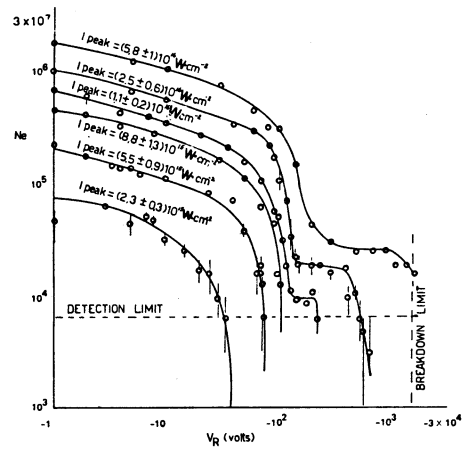


FIG. 8. Electron yield as a function of retarding grid potential with laser peak intensity as a parameter.

as measured from Fig. 8 are plotted as a function of the laser peak intensity and compared with calculated values. In Sec. 3 it was shown that Eq. (3) can be used to estimate the energy of the ejected electrons, assuming instantaneous ejection. For the results shown in Fig. 9, however, a more accurate equation was used that allows for the time variation of the laser pulse during the small, but finite, ejection time. i.e., Eq. (1) is rewritten in the form

$$f_{NL} = -\frac{e^2 E_0^2}{4m_e \omega^2} \nabla [\exp(-2(r/w_0)^2)] H(t, \tau), \quad (7)$$

where E_0 denotes the maximum electric field strength of the beam at $r=0$ and $t=\tau/2$. τ is the total pulse duration, and the function $H(t, \tau)$ determines the time dependence of the laser pulse.

The maximum kinetic energy of electrons initially at a distance r_0 and accelerated to distances $r \gg w_0$ is then given by:

$$\epsilon_{kin} = -\frac{e^2 E_0^2}{4m_e \omega^2} \int_{r_0}^{\infty} H(t, \tau) \nabla [\exp(-2(r/w_0)^2)] dr. \quad (8)$$

The numerical solution of Eq. (8) has been studied by Mavaddat¹⁵ in order to obtain the electron and ion spatial and temporal variations in tenuous plasmas irradiated

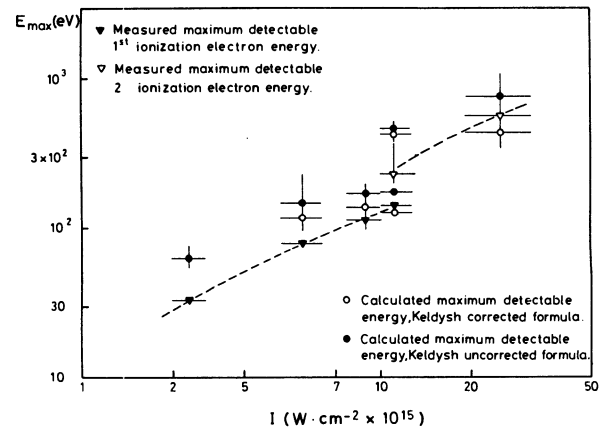


FIG. 9. Maximum detectable electron energy as a function of laser intensity.

ted by intense laser beams with a maximum intensity of 10^{16} W/cm². The laser beam was assumed to be a modified Gaussian in time with $H(t, \tau)$ given by

$$H(t, \tau) = \frac{e^{-k(1-t/\tau)^2} - e^{-k}}{1 - e^{-k}}, \quad 0 \leq t \leq \tau,$$

$$H(t, \tau) = 0, \quad t > \tau,$$

i. e., the beam is modified to make the laser intensity zero at $t=0$ and maximum at $t=\tau/2$.

Equation (8) has also been solved directly¹⁶ to give ϵ_{kin} as a function of the ionization time (Fig. 9) and the laser peak intensity, up to the order of 10^{16} W/cm², assuming a value of $r_0 = 0.1 \mu\text{m}$. Before these results can be applied in the present case, however, they must be modified to allow for the fact that the most energetic electrons that are detected come from the $0.64 I_0$ intensity contour and not the I_0 intensity contour. To estimate the maximum detectable energy, therefore, we make the transformation $I'_0 = 0.64 I_0$ in the solutions for $r_0 = 0.1 \mu\text{m}$, then subtract the contribution to the electron energy from the region $r_0 \leq |r| \leq r'_0$ (where r'_0 is defined by $0.64 I_0 = I_0 \exp\{-2r'^2_0/W^2_{01}\}$), which we assume to be given by

$$\int_{r_0}^{r'_0} \int_{N_L} dr = -\frac{e^2}{4m_e \omega^2} \int_{r_0}^{r'_0} \nabla |E|^2 dr,$$

i. e., the time variation of the ponderomotive force is neglected for $r_0 \leq |r| \leq r'_0$. This will give a good approximation to the upper limit of the maximum detectable energy, since the electrons gain most of their energy in the region $r'_0 \leq |r| \leq r_\infty$ ($r_\infty \gg w_0$).

Good agreement is seen to be obtained in Fig. 9 between the behavior of the calculated maximum values of the maximum detectable electron energy and the measured values, further verifying the existence of the ponderomotive force. It is also seen from Fig. 9 that the calculated values agree more closely with the measured values as the intensity increases. This behavior would be expected, as the model of instantaneous electron ejection assumed in the integration of Eq. (1) becomes more valid as the intensity increases. [It should also be noted, however, that the values for 2.5×10^{16} W/cm² were obtained by extrapolation and should be treated with caution, although they are of the same order as those obtained by direct integration of Eq. (1) over the range $r'_0 \leq |r| \leq r_\infty$ at this intensity, and the two calculations in fact agree to within the accuracy of the quoted errors.]

The second-ionization threshold intensity was obtained even more accurately (Fig. 10). The electron signal is here given as a function of peak intensity with the retarding grid potential as a parameter. At low retarding-grid potentials the detected signal is asymptotic to the calculated curve for the 5.2×10^{14} W/cm² first-ionization threshold intensity. At higher grid potentials (greater than -100 volts) the first-ionization electrons are prevented from reaching the detector and the electron yields are asymptotic to a curve closely approximating that obtained using a threshold intensity value of 4.8×10^{15} W/cm². This value is very much greater than the 9.2×10^{14} W/cm² obtained by Baldwin,¹¹ indi-

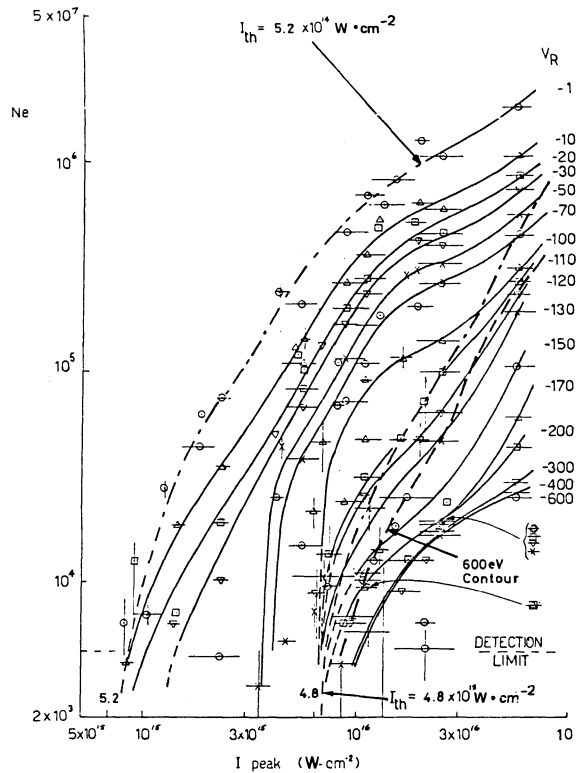


FIG. 10. Electron yield as a function of laser peak intensity with retarding grid potential as a parameter.

cating, as would be expected for $\gamma < 1$, that the ionization is not a multiphoton process. This is supported by later theoretical work, as discussed by Delone *et al.*^{10,16,17}, which suggests that deviation from the multiphoton theory starts at $\gamma^2 < 10$ (linear polarization) or even $\gamma^2 < 15$ (circular polarization).

The measured values of the two ionization thresholds are shown of Fig. 2, where the agreement between the results and the tunneling formula is seen to be very good, with the results favouring agreement with the Keldysh formula uncorrected for long range Coulomb effect. This agreement is most likely the result of two cancelling errors in the Keldysh formula. Manakov and Rapoport¹⁷ in their discussion of the shift and width of a bound level of a particle in a small-radius force field produced by a circularly polarized field show that for $\gamma \leq 1$ the exact solution for the level width differs from the zeroth order approximation. If the width used in the zeroth-order approximation is too great, then the potential barrier width will be reduced and the tunneling probability increased, which for sufficiently strong field gives a result that is too high. For example at $\gamma = 0.8$ Manakov and Rapoport's results¹⁷ differ by a factor 1.5 from the Keldysh results.⁶ If we recall that the Keldysh formulation gives the zeroth-order approximation and also note that the inclusion of the long range Coulomb effects in the Keldysh formulation reduces the ionization probability by a factor of the order of 0.6 (as seen from the computer results given in Fig. 2), then we see that these two effects can be equal and opposite. It would therefore be expected that agreement would be obtained with the uncorrected Keldysh

formulation, rather than the corrected formulation.

The experimental results can also be compared with those of Lompre *et al.*,¹⁸ where experiments were carried out in helium over a small intensity range ($I_0 = (11 \pm 4) \times 10^{14}$ W/cm²) with $\gamma = 0.32$. In this experiment an apparent power-law dependence for the first ionization of helium was measured, in contradiction to both the Keldysh prediction and the results reported here. However, in a similar experiment carried out by Alimov and Delone¹⁹ at $I < 10^{13}$ W/cm² and $\gamma \sim 5$, a similar contradiction was also at first thought to be observed. Alimov and Delone point out, however, that over the small intensity range used in the experiment the dependence of the ionization probability, as calculated from the Keldysh approximation, may be approximated by a power law over this range, giving a value for K that is indistinguishable from the number of photons required for multiphoton ionization, to within the experimental accuracy. Hence the two cases can only be distinguished in this intensity range by measuring the absolute number of electrons or ions produced by ionization and comparing the result with theoretical predictions, as has been done here. This measurement was not carried out by Lompre *et al.* Further, these authors' statement that no transition to saturation was observed in their experiment is exactly consistent with the results presented here, which show that no such transition would be expected, since saturation would have already been achieved over the entire intensity range of their experiment.

Finally, we note from Fig. 10 that at high values of retarding-grid potential, the number of second-ionization electrons measured are considerably less than the expected number calculated for a threshold intensity of 4.8×10^{15} W/cm² and corrected for trapping in the intensity field. Whilst it is expected from Fig. 3 that a spread of energies will occur because the ionization probability is not a true linear function, it is also seen from the same figure that 90% of the electrons would be expected to have energies within the range 350 to 480 eV, assuming instantaneous electron ejection from the focus region. This means that the number of electrons observed with energies less than 480 eV would be expected to be constant and independent of intensity as the intensity is increased. This is indeed observed to be the case for the first ionization electrons, where the energy contours have the same shape as the calculated contour. (It is also seen that the number of electrons with energies less than 52 eV is 20%, i.e., more than would be expected considering Fig. 3 alone; however, it has already been seen that the instantaneous-ejection model is not as good an approximation in this ionization region and that the energies will be somewhat reduced therefore owing to the finite time that the electrons spend in the field, as is seen to be the case.)

Figure 8 also indicates that beyond a retarding grid potential of ~ -350 volts no first-ionization electrons would be expected to be observed. This is consistent with Fig. 10, which indicates little decrease in the number of observed electrons when the retarding potential is increased from -300 to -400 volts. For a

retarding-grid potential of -300 volts, therefore, only a few first-ionization electrons and mostly second-ionization electrons would be expected to be observed. Further, any reduction in the number of electrons observed at -300 to -400 volts would be constant with increasing intensity. This is clearly not the case in Fig. 10, where the number observed varies from $\sim 20\%$ of the calculated number at 10^{16} W/cm² to only $\sim 3\%$ at 6×10^{16} W/cm². Similar behavior is observed with the 600-eV electrons, with the number observed falling away from the expected number as the intensity increases (Fig. 10).

It is possible that some of this loss is due to the axial component of the nonlinear force becoming significant at higher intensities or to secondary electron losses at the detector, and the instrumentation would need to be improved before a definite conclusion could be drawn. We tentatively conclude, however, that at least some of this loss could be caused by a collective photon-electron effect whose strength increases with intensity for intensities greater than $\sim 10^{16}$ W/cm².

5. CONCLUSION

A new experimental technique has been developed for determining the threshold intensities for ionization of a gas. The technique employs the measurement of the energy of ponderomotive force accelerated electrons and provides a means of determining the ionization threshold intensities under conditions where other competing processes are completely absent. Close agreement was obtained between experiment and the theory of Keldysh in the region $\gamma < 1$. The ionization periods in a gas irradiated with a laser beam of peak intensity greater than the threshold intensity and a Gaussian time dependence were also calculated and were found to be several orders of magnitude greater than ω^{-1} for a $1.06 \mu\text{m}$ wavelength beam.

This work has also revealed the possible existence of photon-electron collective effects which impose an axial velocity component on the ejected electrons. Such collective effects may simply be due to the axial ponderomotive force becoming significant above 10^{16} W/cm² at $1.06 \mu\text{m}$. The effect could, however, be due also to entirely new collective interactions of photons and charged particles, the effectiveness of the interaction increasing with the degree of laser-beam focusing and cancelled out at the focus.

Future studies should aim at establishing the existence, or otherwise, of photon-electron collective effects in this field and the determination of the nature of such coupling if it does exist.

The authors wish to thank Mr. P. J. Donohue for excellent technical assistance and Mr. K. G. H. Baldwin, Mr. E. L. Kane, Professor R. Mavaddat and Dr. S. L. Chin for helpful discussion of the work.

¹J. L. Hughes, Recent Developments in Self-Focusing Intense Laser Beams in Dense Plasmas, Invited paper, 6th Vavilov Conference on Nonlinear Optics, Novosibirsk, 20-23 June, 1979 (see also PhD thesis, E. L. Kane, 1979, and PhD

- thesis, V. Del Pizzo 1979, Austral. Nat. Univ.).
- ²F. V. Bunkin and A. E. Kazakov, Dokl. Akad. Nauk SSSR **192**, 71 (1970) [Soviet Physics Doklady **15**, 758 (1971)].
- ³B. W. Boreham, B. Luther-Davies, and J. L. Hughes, Proceedings 9th National Conference on Coherent and Non-Linear Optics, Leningrad, 13–16 June 1978.
- ⁴B. W. Boreham and H. Hora, Phys. Rev. Lett. **42**, 776 (1979).
- ⁵B. W. Boreham and B. Luther-Davies, Journal of Applied Physics **50**, 2533 (1979).
- ⁶L. V. Keldysh, Ionization in the Field of a Strong Electromagnetic Wave, Zh. Eksp. Teor. Fiz. **47**, 1945 (1964) [Sov. Phys. JETP **20**, 1307 (1966)].
- ⁷B. Luther-Davies, Optics Comm. **23**, 98 (1977).
- ⁸M. J. Hollis, Opt. Commun. **25**, 395 (1978).
- ⁹T. P. Hughes, Plasmas and Laser Light, Adam Hilger, Bristol, 1975, p. 50.
- ¹⁰N. B. Delone and V. P. Kraĭnov, Atom v sil'nom svetovom pole (The Atom in a Strong Light Field), Moscow, Atomizdat, 1978, Chapters 4 and 8.
- ¹¹K. G. H. Baldwin, MSc thesis, Australian National University, 1979.
- ¹²Y. P. Raĭzer, Usp. Fiz. Nauk **87**, 29 (1965) [Sov. Phys. Usp. **8**, 650 (1966)].
- ¹³B. W. Boreham, R. Mavaddat, J. L. Hughes, and H. Hora: 11th International Symposium on Rarefied Gas Dynamics, Cannes, France, July 3–8, 1978.
- ¹⁴R. Mavaddat, Journal of Applied Physics (in press).
- ¹⁵N. Delone, G. Delone, V. Gorbunkov, L. Keldysh, M. Rabinovich, and G. Voronov, Proc. 7th Intern. Conf. Phys. Ionized Gases, Belgrade, 1965, p. 177.
- ¹⁶N. Delone, presented at "Europhysics Study Conf. on Multiphoton Processes," Benodet, France, 1979.
- ¹⁷N. L. Manakov and L. P. Rapoport, Zh. Eksp. Teor. Fiz. **69**, 842 (1976) [Sov. Phys. JETP **42**, 430 (1976)].
- ¹⁸L. A. Lompre, G. Mainfray, C. Manus, S. Repoux, and J. Thebault, Phys. Rev. Lett. **36**, 949 (1976).
- ¹⁹D. T. Alimov and N. B. Delone, Zh. Eksp. Teor. Fiz. **70**, 29 (1976) [Sov. Phys. JETP **43**, 15 (1976)].

Saturable absorption and thermal defocusing of light in dye solutions

V. I. Bezrodnyĭ, O. V. Przhonskaya, E. A. Tikhonov, and M. T. Shpak

Physics Institute, Ukrainian Academy of Sciences
(Submitted 16 May 1980)
Zh. Eksp. Teor. Fiz. **80**, 512–523 (February 1981)

The nonlinear transmission (NT) of nanosecond laser radiation ($\lambda = 532\text{nm}$, $\lambda = 694.3\text{nm}$) by molecular solutions of organic dyes is investigated. It is found that at intensities $\approx 10^{25}\text{ cm}^{-2}\text{sec}^{-1}$ the NT of such systems is due to molecular absorption in a system of two or three singlet states, while at intensity higher than $10^{25}\text{ cm}^{-2}\text{sec}^{-1}$ the NT is determined by thermal defocusing. Saturation of the absorption as a result of two-step transitions was observed for molecules with three singlet states, as well as nonstationary thermal self-focusing in the nanosecond time interval.

PACS numbers: 42.65.Jx, 42.60.He, 78.20. — e

Resonant nonlinear absorption of intense light fluxes by complex-molecule solutions is due primarily to the appreciable changes of the populations of the combining states.¹ Many aspects of coherent and nonlinear optics are investigated by the nonlinear-absorption method by varying the frequency, duration, intensity, and coherence of the radiation acting on the investigated object.² A large number of nonlinear-absorption problems involves the use of the nonlinear absorption effect to generate and modulate laser emission,³ to shape light pulses with specified parameters,^{4,5} and for problems of dynamic holography.

A widely used method of studying nonlinear absorption is to measure the waveform of a quasimonochromatic radiation pulse and its energy (power) after passage through a nonlinear absorber. The information obtained in such experiments, particularly the transmission $T = f(I_0, \tau_p, R)$, where I_0 is the intensity at the input, and τ_p and R are the pulse duration and the beam radius in the interaction region, is used to determine the physical picture of the interaction, the energy structure of the molecule, and others.

A number of earlier investigations^{7–10} were made

from approximately this viewpoint. In particular, an analysis^{9,10} of the nonlinear molecular-absorption function $T = f(I_0)$ by the rate-equation method has predicted the existence, in a three-level system, of saturable absorption resulting from two-step transitions (the frequency of the applied radiation was at resonance with the two spin- and symmetry-allowed transitions). Experiment, however, did not yield this result. Furthermore, at high laser-pulse intensities (50–100 MW/cm²) some workers observed a decrease of the nonlinear transmission. It was assumed that this result (the decrease of the nonlinear transmission with increasing pulse energy) was also due to redistribution of the populations of the combining levels^{7,9} and to stimulated light scattering by thermal inhomogeneities of the medium.^{11,12}

We present here the results of the first observation and investigation of the saturation effect due to two-step transitions in molecular solutions of organic dyes. The decrease of the light-scattering-induced nonlinear transmission at high incident-radiation energies is interpreted within the framework of the premises of nonstationary thermal self-focusing.